Version of Record: https://www.sciencedirect.com/science/article/pii/S0010218018304681
Manuscript_02adf50cba8ce4c11c158204c2e72f27

Five kHz Thermometry in Turbulent Spray Flames using Chirped-Probe-Pulse Femtosecond CARS, Part II: Structure of Reaction Zones

Albyn Lowe[1*], Levi M. Thomas[2,] Aman Satija[2], Robert P. Lucht[2] and Assaad R. Masri[1]

[1]School of Aerospace Mechanical and Mechatronic Engineering, The University of Sydney, NSW 2006, Australia
[2]School of Mechanical Engineering, Purdue University, West Lafayette, IN 47906 USA
*Corresponding author: alow2350@uni.sydney.edu.au

Abstract

Temperature was measured in turbulent spray flames of ethanol and acetone stabilized on the piloted Sydney Needle Spray Burner (SYNSBURN^{TM}) using single-laser-shot, chirped-probe-pulse femtosecond coherent anti-Stokes Raman spectroscopy (CPP-fs-CARS) with a repetition rate of 5kHz. The burner features air-blast atomization of liquid injected from a needle that can be translated by a length Lr within a co-flowing air stream so that piloted spray flames ranging from dilute to dense can be studied. Part I of these investigations has reported on the CPP-fs-CARS technique and extensive details of data processing methodology. Part II is concerned with the structure of the reaction zones at different spray loadings and for different departures from blow-off. While not performed simultaneously, measurements of the size distribution of liquid fragments are also reported and discussed in conjunction with the measured temperature. Measured probability density functions of temperature show that for flames with the same liquid loading but different recess lengths, Lr, the near-field spray structure that forms upstream of x/D=10 affects flame structure and stability further downstream. As the spray exiting the burner becomes denser, with a higher proportion of ligaments and 'irregular' shaped objects, the entrainment of hot pilot gases into the spray envelope is affected, hence changing the rates of vaporization and subsequent combustion. The reported results will also form a useful platform for validating sub-models of atomization and combustion in turbulent, dilute to dense spray flames.

Keywords: Temperature measurements; turbulent spray flames; femtosecond-CARS.

© 2018 published by Elsevier. This manuscript is made available under the Elsevier user license
https://www.elsevier.com/open-access/userlicense/1.0/

1. Introduction

Turbulent spray flames remain extremely difficult to compute, particularly for dense or simply non-dilute sprays where non-spherical fragments as well as spherical droplets co-exist and interact over a range of size distributions. This scenario is true for a variety of applications including all direct injection engines and gas turbines. For these systems, close to the injector the liquid fuel is expected to atomize quickly and vaporize forming inhomogeneous but combustible mixtures. This inhomogeneity in composition and liquid fragment distribution will affect, amongst other things, auto-ignition in diesel engines [1–8], stratification in spark-ignition engines [9–11], and stability in gas turbines [12–15]. Understanding the effects of spray structure on the flame remains, therefore, a key challenge, handicapped by the lack of detailed data. One objective of this paper is to provide insights on this issue by presenting new measurements of temperature in turbulent flames of liquid fuels where the spray varies from dilute to dense.

Measurements in spray flames are much more difficult to perform with the same level of detail than in their gaseous counterparts. The presence of liquid fragments makes techniques such as Raman and Rayleigh scattering unworkable, but laser induced fluorescence is still applicable for selected species [16]. Temperature measurement techniques relevant for sprays are limited [17-18] and include NTLAF (non-linear, two-line atomic fluorescence imaging) of indium [19–21], Rainbow methods [22-23], and variants of CARS (coherent anti-Stokes Raman spectroscopy) [24-25]. This paper employs single-laser-shot, chirped-probe-pulse femtosecond coherent anti-Stokes Raman spectroscopy (CPP-fs-CARS) with a repetition rate of 5kHz. This has the advantage of improved spatial resolution over standard CARS and high repetition rates. Details of the application of CPP-fs-CARS and data processing methodology including calibration, relevant corrections and error analysis are presented in earlier publications [26–28].

This paper reports novel information on the measured temperature fields in turbulent spray flames using CPP-fs-CARS. The Sydney piloted spray burner (SYNSBURN^{TM}) is employed to stabilize flames of ethanol or acetone fuels where the spray density ranges from dilute to dense. This variability is achieved through air-blast atomization of liquid injected from a needle that can be translated by a recess length Lr within a co-flowing air stream. The presence of the pilot ensures that the flames are always stabilized onto the burner surface while the spray structure is varied, by manipulating the recess length, Lr. This is a key feature which has already shown that, for the same liquid loading and air-blast conditions, flame stability is indeed affected by the degree of liquid atomization at the jet exit plane as imposed by different Lr [29]. The results of this paper further explore the structure of the reaction zones, as reflected by the temperature measurements, for a suite of sprays flames with range of liquid loading, air blast conditions and recess lengths, Lr.

This simple flow configuration with well-defined boundary conditions is intentionally similar to that employed earlier for studying dilute sprays [30-31]. The international workshop on turbulent combustion of sprays (TCS) [32] has employed this burner to advance the modelling of dilute sprays and the extension to higher spray densities is now feasible with this database provided by the current measurements. The paper is structured as follows: Section 2. Experimental, describes the spray burner (SYNSBURN^{TM}) and the CPP-fs-CARS system located at Purdue University [26–28]. This section also outlines the cases investigated. Sections 3.1 Time Averaged Statistics and 3.2 Temperature-Field Dependence on Spray Inhomogeneity, present the results starting with mean measured profiles of temperature followed by comparisons made by varying liquid loading, airblast velocity and recess length for both acetone and ethanol sprays. Section 3.3 Probability Density Function Analysis, investigates Probability Density Functions of temperature, PDF(T), used to map temperature gradients across the main jet/pilot shear layer interface. In Section 3.4 Temperature and Flow-field Correlation, these findings are linked to flow- and fragment-field characteristics measured separately using Laser Doppler Velocimetry/Phase Doppler Anemometry (LDV/PDA) [29].

2. Experimental

2.1 Burner and Spray Flames

In SYNSBURN^{TM}, spray inhomogeneity is induced by recessing the needle tip relative to the burner surface. The burner, shown schematically in Fig. 1a, uses air-blast to atomize liquid issuing from a needle with a diameter D_l=686μm, centred in a tube with an inner diameter, D=10mm (wall thickness=0.5mm) with a fast co-flowing stream of air. The needle can be recessed by up to 80mm upstream of the jet exit plane. This is similar, in principle, to the gaseous piloted burner which has been used earlier to investigate the effects of inlet compositional inhomogeneity on flame structure [33–35]. The air-blasting jet is surrounded by a pilot with an inner annulus diameter, D_p=25mm, (wall thickness=0.2mm) where premixed hydrogen, acetylene and air issue under stoichiometric conditions with an unburnt velocity U_{bu}=1.5m/s. The pilot composition is such that its C/H ratio is the same as that of the main fuel which is either ethanol or acetone for the spray flames, and provides a respective heat release of 1.60kW and 1.49kW, albeit with a peak adiabatic flame temperature of 2493K and 2512K respectively. This is higher than that of acetone which peaks at 2281K (φ=1.05) and ethanol which peaks at 2355K (φ =1). The entire burner assembly is mounted in a wind tunnel providing a co-flowing air stream with a mean axial velocity of 5m/s.

Fig. 1b displays a selection of flame photographs (both stable and unstable) for a liquid loading of Q=77g/min and a bulk mean air-blast velocity of 60m/s. Five flames are shown from left to right where the recess length is incrementally increased from Lr=0mm to 80mm. Progressing from left to right in Fig. 1b shows how, with increasing recess length, the global spray structure begins to exhibit features of a double reaction zone; with a premixed core and a non-premixed flame surrounding it. This indicates, albeit qualitatively, how substantially different flame structures that span the entire domain from dense to dilute can be obtained by simply varying the recess length.

The parameters controlling flame stability include the recess length, Lr (mm), the liquid mass flowrate, Q (g/min), the air-blast velocity, U_j (m/s), and the contribution of heat release from the pilot. The pilot effects are known from earlier studies of dilute spray flames and are not studied here [36]. The relevant effects of the first three parameters on flame stability are examined in [29]. Global flame instability is qualitatively defined as the 'blow-off' velocity, U_{BO} at which the main flame becomes visibly intermittent and periodically detached from the pilot flame. This generally involves 'necking' of the flame slightly downstream of the pilot and the detection of lighter blue colours as well as a characteristic rumbling sound. Flame stability limits for a) acetone and b) ethanol flames are shown in Fig. 2 plotted against liquid mass loading for different recess lengths of Lr=0mm, 10mm, 25mm and 80mm. Also shown in Fig. 2 are the blow-off velocities, U_{BO} reported by Gounder et al. [30], [36-37] for piloted dilute spray flames of acetone and ethanol (dashed line). The flame on the far left of Fig. 2 which corresponds to zero recess length is blown off as is evident from its colour. This flame is clearly well above the blow-off limit of U_{BO}=53m/s for Q=77g/min as shown in Fig. 2a.

Six spray cases, three for acetone and three for ethanol were chosen for further measurements and selected properties for these are specified in Table 1. The naming methodology is explained with reference to case N-AF8-25 and N-EF2-80: N=Needle, A=Acetone (or E for ethanol), F refers to reacting spray flame and Lr=25 and 80mm respectively. The numerals in AF8 and EF2 refer to cases studied by Gounder et al. [30], [36-37] and employ the same values of Q and U_j. This is intentional as it enables comparisons between established cases of dilute sprays and those studied here. Cases 2 and 6 have the same jet velocity but different liquid loading while the reverse is true for cases 6 and 8. All three cases are marked by boxes in Fig. 2. The exit Weber number, of relevance in this burner, is defined as $We=\rho_g U_g^2 D_l/\sigma$ where ρ_g is the gas density, U_g is the bulk gas velocity and σ is the surface tension. The fuel to air ratio (F/A) listed in Table 1 is defined as the

mass fraction of injected liquid over that of the blast air; and Re_g and Re_l refer to the Reynolds numbers of the carrier air and liquid streams, respectively. Comparisons can be made with jets based on departure from blow-off given the jet velocity ratio U_j/U_{BO}, this is tabulated for fixed recess lengths in Table 1.

2.2 CPP-fs-CARS System

In CPP-fs-CARS, a probe beam is frequency-chirped for single laser shot measurement of the time-dependent frequency spread dephasing of the Raman coherence. The Raman coherence generated by a high-power 800nm beam used as the pump and a tunable 983nm beam used as the Stokes for CARS signal generation from the N_2 Q-branch transitions at ~2330 cm^{-1}. Integration times of less than 4 picoseconds (ps) and spatial resolution of 800 μm along beam propagation and 60 μm in the transverse dimension were achieved. The resulting CARS signal at ~ 675nm is spatially and temporally resolved. The system consists of an amplified titanium-sapphire (Ti:S) fs laser, a frequency shifting optical parametric amplifier (OPA), various routing optics, a calibration flame, a spectrometer and an electron-multiplying charge-coupled device camera (EMCCD). The Ti:S laser (Legend Elite Duo, Coherent Inc) uses chirped-pulse amplification via a pulse stretcher, a regenerative amplifier, a single-pass amplifier, and a compressor to generate 60-fs pulses centred on 800nm at approximately 2mJ per pulse at a 5kHz pulse repetition frequency. A beam-splitter routes 80% of the energy to pump the OPA (OPerA Solo, Coherent Inc.) to create 60-fs Stokes pulses centred on 982nm at 50μJ per pulse. The remaining 20% of the energy is used to generate the pump (100μJ) and probe pulses at a 30-70 energy split respectively. The probe pulse is sent through a chirping rod (30cm SF-10 glass) to impart a frequency dependant delay and stretch the 200μJ pulse from 60-fs to ca. 3.5 ps. Delay stages are used to optimize timing overlap of the pump and Stokes pulses and control the probe time delay. All three beams are focused using a broadband-AR-coated 250mm focal length plano-convex (PCX) lens and are positioned such that their relative geometry satisfies energy and momentum conservation for efficient CARS generation at the probe volume using the “folded-BOXCAR” phase matching protocol. The CARS beam is collected and horizontally dispersed by a 500mm Czerny-Turner-type spectrometer and focused onto a back-illuminated EMCCD camera (iXon888, Andor Technologies). The CARS signal is vertically binned on the EMCCD and the 5kHz laser pulse repetition rate is matched to achieve a 5kHz data acquisition rate. An extended explanation of the CPP-fs-CARS system, calibration and spectral fitting algorithm are found in [26], [38] and are not the focus here. All corrections for interferences detailed in Part I [27] were applied consistently for all spray flame data.

3. Results and discussion

3.1 Time Averaged Statistics

This section presents measured profiles of mean temperature and its rms fluctuations at various axial locations in selected flames listed in Table 1. The intention here is to highlight the effects of fuel loading, air-blast velocity, and fuel type on the temperature fields as measured using CPP-fs-CARS. The results are presented in Fig. 3 and Fig. 4 which have the same layout but showing mean temperature and its rms fluctuations, respectively. In each figure, results are shown for acetone flames AF2, AF6 and AF8 for two recess lengths, namely Lr=80mm which represents dilute spray (left column) and Lr=25mm which is a denser, or moderately dense, spray (middle column). The right column is for ethanol flames EF2, EF6 and EF8 at a recess length Lr=25mm and this provides a good comparison with acetone cases in the middle column. Results are presented for four axial locations of x/D=0.4, 5, 10 and 20 (one x/D per row). Results presented in Fig. 3 and Fig. 4 are discussed jointly. The following observations are made for dilute acetone spray flames AF2, AF6 and AF8 at Lr=80mm (left column of Fig. 3 and Fig. 4):

- The mean temperature profiles are the same for all cases in the near-field region x/D=0.4-5. The twin peak temperatures at these axial locations lie between the physical bounds of the adiabatic temperature of acetone 2281 K and that of the 3-gas pilot 2512 K.
- At x/D=10, the peak mean temperature remains similar, but a radial transition has occurred from flame N-AF8-80 which now shows a narrower radial profile. By x/D=20, this transition has affected the mean peak temperature of AF8 which is now 1650K compared to ~2000K for flames N-AF2-80 and N-AF6-80. This trend is consistent with the proximity to blow-off since flames N-AF2-80 and N-AF6-80 are at U_j/U_{BO}=0.49 and 0.56, respectively while flame N-AF8-80 is closer to blow-off at U_j/U_{BO}=0.75 (see Table 1).
- From x/D~3 to 10, there exists a twin peak in the rms of temperature on each side of the centerline and these correspond to mixing layers at the interfaces of jet/pilot and pilot/coflow. Further downstream at x/D=20, the pilot effects have now subsided and the rms of temperature now peaks on the centerline and on the outer layer where the reaction zone lies. While the peak temperature-rms values are somewhat comparable, flame N-AF6-80 shows slightly higher values which may be partly due to the fact that this flame is in intermediate transition to blow-off at U_j/U_{BO}=0.56.

Comparing now the acetone flame cases N-AF2-25, N-AF6-25 and N-AF8-25, all of which have intermediate spray density (middle column of Fig. 3 and Fig. 4), the following observations are made:

- While at x/D=0.4, all profiles are similar (as was the case for the Lr=80mm flames), the separation starts earlier at x/D=5 and becomes more extreme further downstream. By x/D=10, the peak mean temperature for flames N-AF2-25 and N-AF6-25 is close at ~1700K while that for flame N-AF8-25 is much lower at 1400K. This decrease is also consistent with the proximity to blow-off such that U_j/U_{BO}=0.54, 0.63 and 0.84 for flames N-AF2-25, N-AF6-25 and N-AF8-25, respectively.
- At x/D=20, the peak mean temperatures remain lower than those of the dilute flames (left column at Lr=80mm). The lower peak mean temperature corresponds to flame N-AF8-25 which is closest to blow-off. Note that a slight asymmetry is observed here for flame N-AF2-25.
- Similar to the profiles for the Lr=80mm flames, the rms fluctuations of temperature show twin peaks, albeit less distinct, on either side of the centerline and for x/D=3 to 10. Further downstream at x/D=20, the temperature-rms now peaks on the centerline with the peak rms for flames N-AF6-25 and N-AF8-25 being comparable at ~450K while that for flame N-AF2-25 is higher at 600K.

Flames of acetone and ethanol with Lr=25mm are now compared for cases 2, 6 and 8 (middle and right columns in Fig. 3 and Fig. 4). The following observations are made for these flames of intermediate spray density:

- The trends in the mean temperature profiles are similar for acetone and ethanol fuels. At x/D=10, flames N-AF8-25 and N-EF8-25 have the lowest peak mean temperatures at 1400K and 1500K, respectively. This is consistent with their proximity to blow-off with U_j/U_{BO}=0.84 and 0.8 for acetone and ethanol, respectively. At x/D=20, the profiles for all three ethanol flames are similar and flat with temperatures ~1000K. This implies that the flames are either fully consumed by then or that simply not much burning is taking place while fuel is still present. The latter is probably more realistic.
- The profiles for the rms fluctuations of temperature are also similar for ethanol and acetone flames. However, at x/D=20, the peak rms values for flames N-AF2-25 and N-EF2-25 are 600K and 400K, respectively. This coupled with the lower peak mean temperatures for ethanol flames

at this location implies lower levels of heat release than the acetone counterparts. This is also consistent with ethanol having a lower calorific value (HHV=29.8MJ/kg) and higher boiling point (78°C) than acetone (HHV=31.9 MJ/kg and 56°C).

3.2 Temperature-Field Dependence on Spray Inhomogeneity

This section highlights the effects of varying the recess length, and hence the spray structure on the flame characteristics. Recessing the needle from Lr=0mm to 80mm transitions the spray at the jet exit plane from fully dense to dilute hence changing the stability limits are shown in Fig. 2. The effects of the spray quality on the thermal structure are shown in Fig. 4 which plots profiles of the mean and rms fluctuations of measured temperature for cases N-AF2 and N-EF2. Each plot shows comparison profiles between three recess lengths, namely Lr=0mm, 25mm and 80mm for acetone and Lr=10mm, 25mm and 80mm for ethanol. The two columns on the left are for acetone mean temperature and rms fluctuations while the two on the right are for ethanol. The following points are noted:

- At upstream locations down to x/D=5, the recess length has little or no effect on the mean thermal structure. This is expected since within this region the flame is dominated by the pilot; the bulk of the spray is close to the jet centerline, and hence the quality of spray does not have much impact on the reaction zone. This is also supported by the mean centerline temperatures being mostly the same for recess lengths 25mm and 80mm.
- Further downstream at x/D=10, and 20, it is evident that, for the same liquid loading and airblast condition, the recess length does have an impact and the higher proportion of fragments and filaments present at lower Lr, lead to less stable flames as reflected in the lower mean temperatures. Note also that for ethanol, the mean and rms fluctuations for the dilute case (Lr=80mm) are much higher than those of Lr=10 and 25mm, implying that burning is still sustained at this downstream location unlike the latter two cases which seem to have extinguished.
- By decreasing the recess length, the residence time within the airblast tube upstream of the jet exit plane decreases and this diminishes the degree of fuel vaporization within the tube. Therefore, at lower Lr there are more liquid fragments within the pilot stream and these evaporate thereby removing heat from the pilot gases. This is evident in the mean temperature profiles at x/D=5 for N-EF2-10 and particularly N-AF2-0 where the peak values are colder for the dense case. For the dilute cases, the pre-vaporization of fuel results in colder temperatures on the inside of the pilot. This is less pronounced for lower Weber number cases and particularly for ethanol which atomizes less than acetone in the near-field.

3.3 Probability Density Function Analysis

The high repetition of the CPP-fs-CARS system (5kHz) rate enables the acquisition of a large number of data points and hence the generation of probability density functions of temperature PDF(T). These may be plotted for a range of radial locations so that one can see the evolution of the PDF in space. Similarly, the PDF(T) for a range of flames approaching blow-off or having a different recess length, Lr shows how the spray structure affects temperature distribution and hence local reaction zones. This section presents and discusses a series of PDF(T) plots for acetone flames AF2, AF6 and AF8 as well as ethanol flame EF2 which is compared with AF2. The rest of the data is not shown here but are tabulated in the spray database and will be made available on request.

The PDF(T)s measured at various axial and radial locations in flames AF2, AF6, and AF8, and EF2 are displayed in Fig. 6-Fig. 9 respectively and each position is labelled (a)-(x). For each figure, a row corresponds to a specific radial location and shows plots for x/D=0.4, 5, 10 and 20. Six rows of data are shown in each figure corresponding to increasing radial locations from r/D=0 (bottom row) to r/D=1.4 (top row). Each plot shows up to three PDF(T)s for three different recess lengths of

Lr=0mm, 25mm and 80mm. These are indicated on each plot, for example: N-AF2-80|25|0 correspond to a comparison between N-AF2-80, N-AF2-25, N-AF2-00 respectively. Three vertical lines are demarcated on each plot depicting (i) room temperature (298K), (ii) adiabatic temperature of the acetone or ethanol (2281K and 2355K respectively), and (iii) the adiabatic temperature of the 3-gas pilot (2512K for acetone and 2493K for ethanol). Temperatures above the physical bounds of the adiabatic temperature of the liquid fuel are attributed to the premixed 3-gas pilot and are not a point of interest here when interpreting spray combustion.

The mean, $\bar{T}$, and rms of temperature, σ_T, are presented on each PDF plot with the respective r/D locations: for example the PDF labelled (j) in Fig. 6 at x/D=5 (second column), N-AF2-80 at r/D=0.8 (third row from top) has $\bar{T}$=1982K and σ_T=127K, N-AF2-25 at r/D=0.7 has $\bar{T}$=1827K and σ_T=260K, N-AF2-0 at r/D=0.8 has $\bar{T}$=1379K and σ_T=558K. In all these plots, traverse from left to right to observe downstream axial locations (x/D=3-20) and scan from top to bottom to radially approach the centerline of the flame. Results are now discussed collectively for the acetone cases (N-AF2-80|25|0 (Fig. 6) N-AF6-80|25 (Fig. 7) and N-AF8-80|25 (Fig. 8). Ethanol case N-EF2-80|25|10 (Fig. 9) is provided for comparisons of fuel type. The following observations made in these bullet points are for all cases reported in Fig. 6-Fig. 9 unless specified otherwise.

- At (a) x/D=0.4 on the centerline, the PDF's are narrow and centered at the liquid temperature, as expected. As the pilot is traversed at r/D=0.6 through to 1.2 (c)-(e), the PDF's shift to peak around the pilot temperature of 2512K and 2493K respectively for acetone and ethanol. Further out at (f) r/D=1.4, the probe is in the outer pilot/air and the temperature decreases. At this axial location, the recess length does not seem to have much impact on the PDF except for slight radial variations in the mixing layer at the pilot/fuel (r/D=0.5) and pilot/air interfaces (r/D=1). These comments are consistent for all cases reported in Fig. 6-Fig. 9.
- At (g) x/D=5 and the centerline, the PDF's still match the liquid temperature and then increase at (h) r/D=0.4. However, at (i) and (k) defined as r/D=0.6 and 1.2 in the acetone flames, temperature distributions for the Lr=25mm cases are lower than those for the dilute cases at Lr=80mm. Specifically at (j) r/D=0.8, the dilute cases with Lr=80mm show peak temperatures slightly lower than that of the pilot and this decreases gradually with recess lengths of Lr=25mm and 0mm. It is noted that at this upstream axial location, the pilot gases may still be having an impact, but increasing the spray density (at Lr=25mm and 0mm) reduces the overall proportion of burnt samples. Noting also that this effect is less distinct for ethanol as shown in Fig. 9.
- At (m) x/D=10, this cooling effect caused by decreasing the recess length has further developed across the radial expanse of (o)-(q) r/D=0.6-1.2. The high temperatures of ~1800K to 2000K observed mainly for Lr=80 (at r/D=0.8 and 1.2) cases are indicative of almost fully burnt fluid. It is also worth noting that at this downstream location, the effects of the pilot are minimal as is evident from the shift in peak temperatures. The broad profiles shown at (o) r/D=0.6 of Fig. 7 highlight why the rms fluctuations of temperature (as seen in the rms profile in Fig. 4) peak at this radial location for flames N-AF6-25 and N-AF6-80. Flame N-AF6-80 transitions to full burning at (p) r/D=0.8 while flame N-AF6-25 remains only partly burnt with colder samples persisting at r/D=0.8. At this downstream location the temperature profiles appear more sensitive to the effects of recess length. The centerline temperatures are also warmer as shown from (m)-(n) the bottom rows of this column.
- Continuing to (s)-(x) x/D=20, the centerline PDF's begin to display burning samples and the trends exhibited at x/D=10 develop across the entire spray cross section. Decreasing the recess length increases the temperature on the centerline noticeably as seen from the plots labelled (s) in the bottom row. For example, for (s) in Fig. 8 the peak of the pre-heated vapor temperature distribution for N-AF8-80 is consistently colder than for N-AF8-25 with values of 680K and 600K, respectively at x/D=20. By this downstream location, there persists cold room

temperature samples in the dilute case (Lr=80mm). On the contrary, for a recess length of 25mm at x/D=20, room air temperatures do not exist and the hot burnt gases approach temperatures close to the adiabatic temperature of the acetone fuel, which is 2281 K. For ethanol, this effect is similar but delayed such that in Fig. 9, N-EF2-80 deviates from the N-EF2-25 case only at x/D=20. The cold room air is not present in the dilute ethanol case and perhaps indicates a lower degree of dispersion for the less viscous fuel at centerline locations. This can be attributed to lower Weber number for the ethanol droplets.

- The degree of vaporization and mixing on centerline in ethanol spray flames is clearly lower than for the acetone spray flames at the same conditions. It is also evident from the PDF's shown in Fig. 9 that differences with recess length are less distinct (except for x/D=20) than those observed for acetone. This may be due to combinations of reasons which could possibly include the lower volatility and hence lower dispersion of ethanol. Ethanol has a dynamic viscosity of 1.19E-04kg/ms as oppose to acetone at 3.33E-04kg/ms. It is also worth noting that this is consistent with the changes in stability limits and the data reported in Table 1 where with increasing Lr, acetone flames approach blow-off at a quicker rate than ethanol counterparts.

From these observations, three characteristic peaks exist in the temperature distributions ordered from coldest to hottest: 1) room air, 298 K 2) pre-heated vapor, 500-750 K and 3) burnt gases, 1500 K to T_{ad} of the fuel. The spatial distribution of the cold air samples is greatest on centerline and dissipates radially up to r/D=0.4. Strong peaks in pre-heated vapor in the presence of hot burnt gases dominate the axial expanse at r/D=0.6 and the radial expanse of x/D=20 in dilute spray flames (recess length 80mm). These distributions, bimodal for dilute cases and right-hand skewed for dense cases, outline the spatial bounds of the potential core in the spray flame; a representation of the turbulent reaction zone.

3.4 Temperature and Flow-field Correlation

Insight into spray flame structure and the inhomogeneous combustion can be gained from comparisons between the temperature- and flow-field measurements even if those are not performed simultaneously. The flow-field measurements were performed earlier in the same flames using LDV/PDA [29] to obtain probability density functions of droplet sizes, herein PDF(D), at similar locations in the spray flames. The samples are restricted to spherical droplet diameters in the size range of 2-110μm. Even though these measurements are not simultaneous, the analysis presented here provide useful physical insights. For example, it is shown that the PDF(D) does not vary significantly from x/D=10-20, while the PDF(T) does. This implies that these flames are influenced by the spray structure that forms upstream of x/D=10. Here are further details.

Displayed in Fig. 10 and Fig. 11 are comparisons of the measured probability density functions of temperature, PDF(T), and droplet size distribution, PDF(D), for selected combinations of acetone flames. Fig. 10 shows comparisons for flames with different recess lengths of Lr=80mm, 25mm and 0mm for flame AF2 (N-AF2-80|25|0) while Fig. 11 compares the effect of the three dilute cases for Lr=80, N-AF2-80, N-AF6-80 N-AF8-80 (labelled as N-AF2|6|8-80). The plots labelled (a)-(l) are laid out similarly in Fig. 10 and Fig. 11 as follows: the PDF(T) from CPP- fs-CARS are presented in rows 2 and 4 from the bottom for x/D=10 and 20, respectively. The PDF(D) from LDV/PDA are provided in rows 1 and 3 from the bottom for x/D=10 and 20, respectively. Traverse from right to left decreases r/D=0.8 to zero, to radially approach the centerline of the flame. Conceptually, the first column represents the rich limit at the centerline of the spray jet, the second column is close to r/D=0.6 which at x/D=5 corresponds to the location where the mean reaction zone appears to exist as indicated by the mean temperature profiles in Fig. 3 and Fig. 5; and finally, the third column represents the lean limit and the radial extent at which droplet size measurements are detectable by the LDV/PDA system.

The correlations between temperature and droplet size in acetone spray flames with varying recess length are presented for N-AF2-80|25|0 (Fig. 10). For PDF(T)s, the format of the mean, $\bar{T}$, and rms of temperature, σ_T, follows that for spray flames where the recess length varies, as explained in Fig. 6-Fig. 9. For PDF(D)s, the arithmetic mean droplet size, D_{10}, and standard deviation of droplet size, $\sigma_{D,}$ presented right side of each PDF plot with the respective r/D location on the top left corner: for example in (i) Fig. 10, at x/D=10 (first row from bottom) N-AF2-80 at r/D=0.8 (third column) has D_{10}=37μm and σ_D=21μm, N-AF2-25 at r/D=0.8 has D_{10}=38μm and σ_D=20μm, N-AF2-0 at r/D=0.8 has D_{10}=37μm and σ_D=20μm. In all these plots, traverse from right to left to radially approach the centerline of the flame and scan from bottom to top to observe downstream axial locations (x/D=10-20). Comparisons for dilute spray cases N-AF2|6|8-80 are displayed in Fig. 11 respectively. For PDF(D)s, the arithmetic mean droplet size, D_{10}, standard deviation of droplet size, σ_D and respective r/D location are adjusted such that at (i) Fig. 11, x/D=10 (first row from bottom) N-AF2-80 at r/D=0.8 (third column) has D_{10}=37μm and σ_D=21μm, N-AF6-80 at r/D=0.8 has D_{10}=38μm and σ_D=21μm and N-AF8-80 at r/D=0.72 has D_{10}=36μm and σ_D=21μm.

With the qualifier that PDF(D) and PDF(T) are not measured simultaneously, the following observations are made with respects to the results presented here:

- The trends in Fig. 10 clearly show that the recess length greatly affects the thermal structure of these spray flames. For this comparison of recess length, the velocity ratio marking proximity to blowoff is U_j/U_{BO}=0.49, 0.54 and 0.68 for N-AF2-80, N-AF2-25 and N-AF2-0 respectively and this specific case is steady with a high degree of mixing. For a recess length of 25mm, the PDF(T) distribution shows two peaks, the hotter of the two is characteristic of pre-heated vapor and the colder sub-298K peak. The dense spray flame with Lr=0mm shares a similar distribution as the Lr=25mm case albeit with fewer samples below room temperature. This trend with recess length is consistent amongst all flame cases.
- In terms of the flow-field in Fig. 10, the PDF(D) at (a)-(d) r/D=0 and (i)-(l) ~0.8 display the same distribution for all recess lengths with a steady arithmetic mean droplet size D_{10} of 35-40μm and standard deviation of 20μm. This observation holds in all the flame cases irrespective of recess length, when the spray is burning and temperatures are consistently above 1000K in the PDF(T). At these locations, the thermal structure of the spray flames is independent of the droplet size distribution ranging 2-110μm. The mean droplet size value does not appear to dictate the thermal structure of these spray flames.
- Large liquid fragments characteristically modulate the flow-field which can reduce the mixing of fuel and oxidizer. This may explain why significantly fewer samples >1500 K for the colder 25mm and 0mm recess cases exist. The addition of spray flame inhomogeneity reduces the rms value of temperature (f) and (h) at r/D=0.5-0.6 for all the flame cases.
- In Fig. 11, the peak of the PDF(D), for example in (c), trends with Weber number such that N-AF8 typically has the highest value of small droplet diameter sizes and N-AF2 generally follows N-AF6. Regardless of recess length or Weber number, the PDF(T) trends with F/A ratio, for example in (h), where N-AF2 is hottest and N-AF8 the coldest.

Axial scans of the mean measured temperature and Sauter mean diameter, D_{32} are presented in Fig. 12 labelled (a)-(r) for radial locations r/D=0 (left column), 0.4 (center) and 0.6 (right column) in selected spray flames of acetone. The top two rows of plots compare mean temperature (row 1) and, D_{32} (row 2) for AF2 at three recess lengths of Lr=0mm, 25mm and 80mm. The middle two rows show similar layout of comparisons but now for flame N-AF6-25 and N-AF6-80 while the bottom two rows compare AF8 with also two recess lengths, namely flame N-AF8-25 and N-AF8-80. It is noted that the plots for D_{32} (rows 2, 4, and 6 from the top) also show additional data for the fully dilute cases AF2, AF6 and AF8 as obtained from Gounder et al. [37] (this data is plotted with asterisks).

Regarding r/D=0 in the left column only, the trend in (a), (g) and (m) centerline D_{32} shows that increasing the recess length significantly increases the degree of vaporization predominantly for axial lengths less than x/D=10, where higher SMD values exist for lower recess length. This effect is clearer for cases with higher fuel loadings, for example at x/D=5, D_{32}=50, 56 and 63μm for (m) N-AF2-80|25|0, while D_{32}=45 and 48μm for (g) N-AF6-80|25. Although subtle in (d), (j) and (p) the mean centerline temperature is generally higher for the cases with lower recess length below x/D=10. These two features indicate the enhanced evaporation of fuel and turbulent mixing with ambient air for dilute flames. For a recess length of 25mm, the CARS temperature measurements are higher and do not include samples close to room air temperatures as verified in centerline PDF(T)s in Fig. 6-Fig. 8.

At outer radial locations away from the centerline (middle and right column), the D_{32} values remain well-grouped despite changing the recess length and increase slightly by ~5-10μm further downstream from x/D=0.4-20. The temperature measurements behave differently whereby traversing radially results in dilute cases displaying hotter values when compared to their denser counterparts. In the middle column where r/D=0.4, the D_{32} profile does not vary axially for different recess length while the temperature begins to vary by x/D=10. By r/D=0.6 in the right column, the temperature profiles vary at all axial locations while the D_{32} does not. This is true except for the fully dilute cases from [37] which show lower D_{32} values upstream of x/D=20. It is clear from these observations that the effect of recess length on temperature does not make a difference upstream of x/D=10 and close to the spray jet but does come into significant effect further downstream and at outer radial locations initiating at r/D=0.6.

4. Conclusions

Analysis of the temperature data acquired using CPP-fs-CARS has provided insight into the structure of turbulent sprays flames spanning the entire range from dilute to dense and for different departures from blow-off. Comparisons with measurements of droplet-field distributions are useful even though these were not made simultaneously with temperature. The following conclusions are drawn:

- Increasing the recess length in these spray flames significantly alters the thermal structure of the reaction zones downstream and this is isolated to the influence of ligaments and ‘irregular’ shaped objects in abundance in the near-field.
- These large liquid bodies affect the entrainment of hot pilot gases into the spray envelope upstream of x/D=10.
- This effect is clearly depicted in point temperature PDFs highlighted by the transition from bimodal distributions of preheated vapor and burnt gases in dilute flames to skewed distributions in denser flames. By inference the compositional structure would also change and this will be alluded to in future measurements.

The data presented promises to be a rigorous platform for validating and improving the modelling of various aspects of turbulent sprays flames with compositional inhomogeneity and varying liquid loading densities.

5. Acknowledgements

The University of Sydney Combustion Group is supported by the Australian Research Council. The Department of Mechanical Engineering at Purdue University was supported by a fellowship from the Purdue Military Research Initiative. Funding was provided by the U.S. Department of Energy, Division of Chemical Sciences, Geosciences and Biosciences, Grant No. (DE-FG02-03ER15391) and by the King Abdullah University of Science and Technology, CCF subaward (No.1975-01).

6. References

[1] C. Bajaj, M. Ameen, and J. Abraham, Evaluation of an unsteady flamelet progress variable model for autoignition and flame lift-off in diesel jets, Combust. Sci. Technol. 185 (2013) 454–472

[2] R. N. Dahms, J. Manin, L. M. Pickett, and J. C. Oefelein, Understanding high-pressure gas-liquid interface phenomena in diesel engines, Proc. Combust. Inst. 34 (2013) 1667–1675

[3] N. Abani, A. Munnannur, and R. D. Reitz, Reduction of Numerical Parameter Dependencies in Diesel Spray Models, J. Eng. Gas Turbines Power 130 (2008) 032809–032809

[4] M. R. Turner, S. S. Sazhin, J. J. Healey, C. Crua, and S. B. Martynov, A breakup model for transient Diesel fuel sprays, Fuel 97 (2012) 288–305

[5] J. Shinjo and A. Umemura, Detailed simulation of primary atomization mechanisms in Diesel jet sprays (isolated identification of liquid jet tip effects), Proc. Combust. Inst. 33 (2011) 2089–2097

[6] K. Kim, D. Kim, Y. Jung, and C. Bae, Spray and combustion characteristics of gasoline and diesel in a direct injection compression ignition engine, Fuel 109 (2013) 616–626

[7] A. Kourmatzis, P. X. Pham, and A. R. Masri, Air assisted atomization and spray density characterization of ethanol and a range of biodiesels, Fuel 108 (2013) 758–770

[8] A. Kastengren, C. F. Powell, Z. Liu, and J. Wang, Time resolved, three-dimensional mass distribution of diesel sprays measured with X-ray radiography, SAE Tech. Pap. Ser. (2009)

[9] A. R. Masri, Partial premixing and stratification in turbulent flames, Proc. Combust. Inst. 35 (2015) 1115–1136

[10] B. Peterson, E. Baum, B. Böhm, V. Sick, and A. Dreizler, Spray-induced temperature stratification dynamics in a gasoline direct-injection engine, Proc. Combust. Inst. 35 (2015) 2923–2931

[11] Y. Yang, J. E. Dec, N. Dronniou, and M. Sjöberg, Tailoring HCCI heat-release rates with partial fuel stratification: Comparison of two-stage and single-stage-ignition fuels, Proc. Combust. Inst. 33 (2011) 3047–3055

[12] J. E. Temme, P. M. Allison, and J. F. Driscoll, Combustion instability of a lean premixed prevaporized gas turbine combustor studied using phase-averaged PIV, Combust. Flame 161 (2014) 958–970

[13] S. K. Dhanuka, J. E. Temme, and J. F. Driscoll, Lean-limit combustion instabilities of a lean premixed prevaporized gas turbine combustor, Proc. Combust. Inst. 33 (2011) 2961–2966

[14] B. Janus, A. Dreizler, and J. Janicka, Experiments on swirl stabilized non-premixed natural gas flames in a model gasturbine combustor, Proc. Combust. Inst. 31 (2007) 3091–3098

[15] C. D. Slabaugh, C. N. Dennis, I. Boxx, W. Meier, and R. P. Lucht, 5 kHz thermometry in a swirl-stabilized gas turbine model combustor using chirped probe pulse femtosecond CARS. Part 2. Analysis of swirl flame dynamics, Combust. Flame 173 (2016) 454–467

[16] J. Desantes, J. Pastor, J. Pastor, and J. Julia, Limitations on the use of the planar laser induced exciplex fluorescence technique in diesel sprays, Fuel 84 (2005) 2301–2315

[17] F. Beyrau, A. Bräuer, T. Seeger, and A. Leipertz, Gas-phase temperature measurement in the vaporizing spray of a gasoline direct-injection injector by use of pure rotational coherent anti-Stokes Raman scattering, Opt. Lett. 29 (2004) 247–249

[18] S. R. Engel et al., Gas phase temperature measurements in the liquid and particle regime of a flame spray pyrolysis process using O2-based pure rotational coherent anti-Stokes Raman scattering., Appl. Opt. 51 (2012) 6063–6075

[19] P. R. Medwell, Q. N. Chan, B. B. Dally, S. Mahmoud, Z. T. Alwahabi, and G. J. Nathan, Temperature measurements in turbulent non-premixed flames by two-line atomic fluorescence, Proc. Combust. Inst. 34 (2013) 3619–3627

[20] J. Trost, L. Zigan, and A. Leipertz, Quantitative vapor temperature imaging in DISI-sprays at elevated pressures and temperatures using two-line excitation laser-induced fluorescence, Proc. Combust. Inst. 34 (2013) 3645–3652

[21] P. R. Medwell, A. R. Masri, P. X. Pham, B. B. Dally, and G. J. Nathan, Temperature imaging of turbulent dilute spray flames using two-line atomic fluorescence, Exp. Fluids 55 (2014) 1840
[22] P. Lemaitre, E. Porcheron, G. Grehan, and L. Bouilloux, Development of a global rainbow refractometry technique to measure the temperature of spray droplets in a large containment vessel, Meas. Sci. Technol. 17 (2006) 1299
[23] S. Saengkaew, G. Godard, J. B. Blaisot, and G. Gréhan, Experimental analysis of global rainbow technique: sensitivity of temperature and size distribution measurements to non-spherical droplets, Exp. Fluids 47 (2009) 839
[24] S. Roy, J. R. Gord, and A. K. Patnaik, Recent advances in coherent anti-Stokes Raman scattering spectroscopy: Fundamental developments and applications in reacting flows, Prog. Energy Combust. Sci. 36 (2010) 280–306
[25] A. M. Zheltikov, Coherent anti-Stokes Raman scattering: from proof-of-the-principle experiments to femtosecond CARS and higher order wave-mixing generalizations, J. Raman Spectrosc. 31 (2000) 653–667
[26] L. M. Thomas, A. Satija, and R. P. Lucht, Technique developments and performance analysis of chirped-probe-pulse femtosecond coherent anti-Stokes Raman scattering combustion thermometry, Appl. Opt. 56 (2017) 8797–8810
[27] L. M. Thomas, A. Lowe, A. Satija, R. P. Lucht, and A. R. Masri, 5kHz Thermometry in Turbulent Spray Flames Using Chirped-Probe-Pulse Femtosecond CARS, Part 1: Processing and Error Analysis (2018) doi: 10:1016/j.combustflame.2018.06
[28] A. Lowe, L. M. Thomas, A. Satija, R. P. Lucht, and A. R. Masri, Chirped-probe-pulse femtosecond CARS thermometry in turbulent spray flames, Proc. Combust. Inst. 37 (2018) doi: 10.1016/j.proci.2018.06.149
[29] A. Lowe, A. Kourmatzis, and A. R. Masri, Turbulent spray flames of intermediate density: Stability and near-field structure, Combust. Flame 176 (2017) 511–520
[30] S. H. Stårner, J. Gounder, and A. R. Masri, Effects of turbulence and carrier fluid on simple, turbulent spray jet flames, Combust. Flame 143 (2005) 420–432
[31] A. R. Masri and J. D. Gounder, Details and Complexities of Boundary Conditions in Turbulent Piloted Dilute Spray Jets and Flames, Experiments and Numerical Simulations of Diluted Spray Turbulent Combustion, Springer, Dordrecht, 2011, pp. 41–68.
[32] http://www.tcs-workshop.org/ [Accessed: 05-Apr-2017].
[33] R. S. Barlow, S. Meares, G. Magnotti, H. Cutcher, and A. R. Masri, Local extinction and near-field structure in piloted turbulent CH4/air jet flames with inhomogeneous inlets, Combust. Flame 162 (2015) 3516–3540
[34] S. Meares and A. R. Masri, A modified piloted burner for stabilizing turbulent flames of inhomogeneous mixtures, Combust. Flame 161 (2014) 484–495
[35] S. Meares, V. N. Prasad, G. Magnotti, R. S. Barlow, and A. R. Masri, Stabilization of piloted turbulent flames with inhomogeneous inlets, Proc. Combust. Inst. 35 (2015) 1477–1484
[36] A. R. Masri and J. D. Gounder, Turbulent spray flames of acetone and ethanol approaching extinction, Combust. Sci. Technol. 182 (2010) 702–715
[37] J. D. Gounder, A. Kourmatzis, and A. R. Masri, Turbulent Piloted Dilute Spray Flames: Flow Fields and Droplet Dynamics, Combust. Flame 159 (2012) 3372–3397
[38] C. N. Dennis, C. D. Slabaugh, I. G. Boxx, W. Meier, and R. P. Lucht, Chirped probe pulse femtosecond coherent anti-Stokes Raman scattering thermometry at 5 kHz in a Gas Turbine Model Combustor, Proc. Combust. Inst. 35 (2015) 3731–3738

Table of Figures

Fig. 1 – a) Cross-section schematic of atomizer and burner assembly showing the pilot stream (1), main air jet stream (2) and liquid fuel stream (3). b) Sample long exposure (1s) images of the acetone flames for a mass loading of Q=75g/min and U_j=60m/s at various recess lengths. 3

Fig. 2 – Blow-off air-blast jet velocity (U_{BO}) plotted vs. liquid acetone mass loading (Q) as a function of recess length (Lr). Dashed line corresponds to equivalent dilute sprays from Gounder et al. [30], [36-37] and boxes specify selected cases defined in Table 1 for a) acetone and b) ethanol. 4

Fig. 3 – Radial profiles of the mean temperature measured at various axial locations using the CPP-fs-CARS system. Profiles are plotted for reacting acetone spray flames N-AF2, N-AF6 and N-AF8 comparing recess lengths 80 and 25mm. $T_{ad,C3H6O}$ = 2281K and $T_{ad,3GP}$ = 2512K. Alternatively, reacting ethanol spray flames N-EF2, N-EF6 and N-EF8 for recess length 25mm. $T_{ad,C2H6O}$ = 2355K and $T_{ad,3GP}$ = 2493K. 7

Fig. 4 – Radial profiles of the rms of temperature measured at various axial locations using the CPP-fs-CARS system. Profiles are plotted for reacting acetone spray flames N-AF2, N-AF6 and N-AF8 comparing recess lengths 80 and 25mm. $T_{ad,C3H6O}$ = 2281K and $T_{ad,3GP}$ = 2512K. Alternatively, reacting ethanol spray flames N-EF2, N-EF6 and N-EF8 for recess length 25mm. $T_{ad,C2H6O}$ = 2355K and $T_{ad,3GP}$ = 2493K. 8

Fig. 5 – Radial profiles of the mean and rms of temperature measured at various axial locations using the CPP-fs-CARS system. Profiles are plotted for reacting acetone and ethanol spray flames comparing recess length N-AF2-80/N-EF2-80, N-AF2-25/N-EF2-25 and N-AF2-0/N-EF2-10. For acetone, $T_{ad,C3H6O}$ = 2281K and $T_{ad,3GP}$ = 2512K; for ethanol, $T_{ad,C2H6O}$ = 2355K and $T_{ad,3GP}$ = 2493K. 10

Fig. 6 – Spatial mapping of temperature PDF(T) using the CPP-fs-CARS for N-AF2-80 (solid), N-AF2-25 (dash) and N-AF2-0 (dot). Room temperature, $T_{ad,C3H6O}$ = 2281K and $T_{ad,3GP}$ = 2512K demarcated as vertical lines. 11

Fig. 7 – Spatial mapping of temperature PDF(T) using the CPP-fs-CARS for N-AF6-80 (solid) and N-AF6-25 (dash). Room temperature, $T_{ad,C3H6O}$ = 2281K and $T_{ad,3GP}$ = 2512K demarcated as vertical lines. 12

Fig. 8 – Spatial mapping of temperature PDF(T) using the CPP-fs-CARS for N-AF8-80 (solid) and N-AF8-25 (dash). Room temperature, $T_{ad,C3H6O}$ = 2281K and $T_{ad,3GP}$ = 2512K demarcated as vertical lines. 13

Fig. 9 – Spatial mapping of temperature PDF(T) using the CPP-fs-CARS for N-EF2-80 (solid), N-EF2-25 (dash) and N-EF2-10 (dot). Room temperature, $T_{ad,C2H6O}$ = 2355K and $T_{ad,3GP}$ = 2493K demarcated as vertical lines. 15

Fig. 10 – Temperature, PDF(T) and flow-field PDF(D) correlation for N-AF2-80 (solid), N-AF2-25 (dash) and N-AF2-0 (dot). Room temperature, $T_{ad,C3H6O}$ = 2281K and $T_{ad,3GP}$ = 2512K demarcated as vertical lines. 17

Fig. 11 – Temperature, PDF(T) and flow-field PDF(D) correlation for N-AF2-80 (solid), N-AF6-80 (dash) and N-AF8-80 (dot). Room temperature, $T_{ad,C3H6O}$ = 2281K and $T_{ad,3GP}$ = 2512K demarcated as vertical lines. 18

Fig. 12 – Axial profiles at r/D=0, 0.4 and 0.6 (left, middle, right columns respectively) of the mean temperature (T, 1^{st}, 3^{rd}, 5^{th} rows from top) measured using the CPP-fs-CARS system and Sauter mean diameter (D_{32}, 2^{nd}, 4^{th}, 6^{th} row) measured using the PDA system. Profiles are plotted for reacting acetone spray flames comparing recess lengths. For acetone, $T_{ad,C3H6O}$ = 2281K and $T_{ad,3GP}$ = 2512K. 20

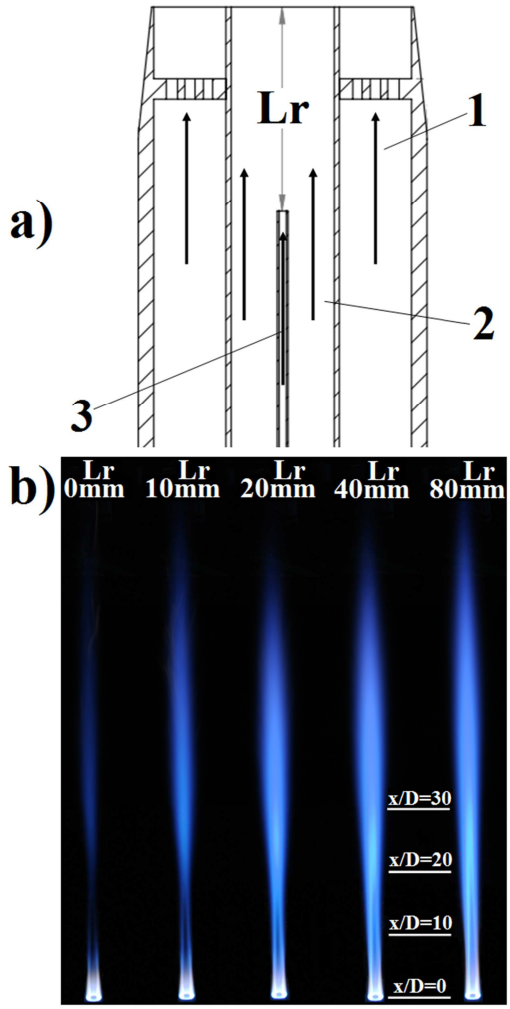

Fig. 1 – a) Cross-section schematic of atomizer and burner assembly showing the pilot stream (1), main air jet stream (2) and liquid fuel stream (3). b) Sample long exposure (1s) images of the acetone flames for a mass loading of Q=75g/min and U_j=60m/s at various recess lengths.

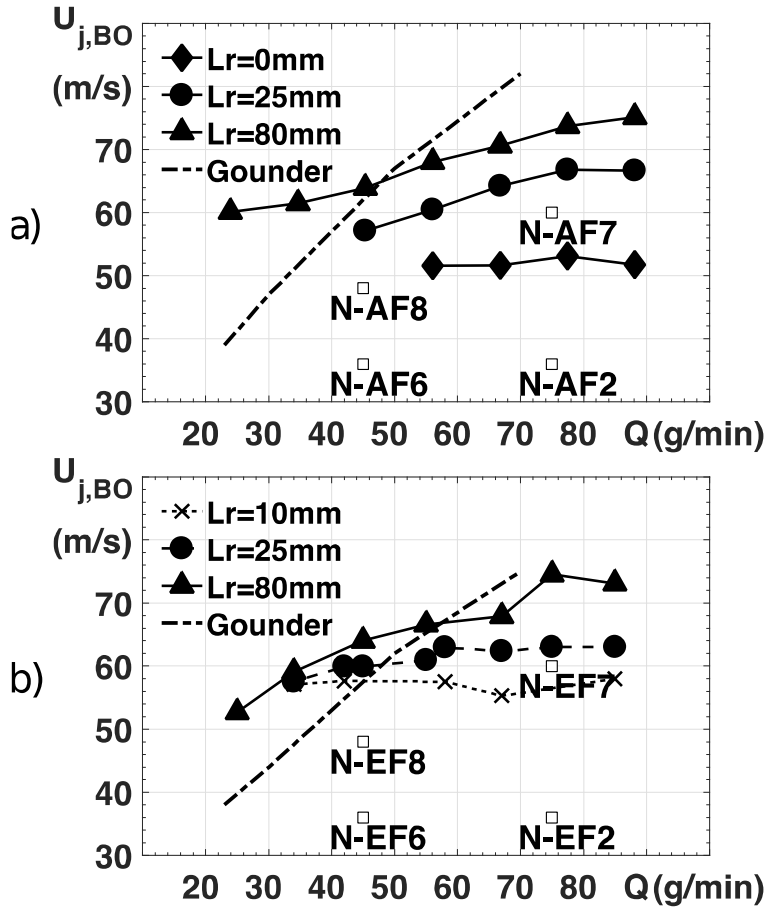

Fig. 2 – Blow-off air-blast jet velocity (U_{BO}) plotted vs. liquid acetone mass loading (Q) as a function of recess length (Lr). Dashed line corresponds to equivalent dilute sprays from Gounder et al. [30], [36-37] and boxes specify selected cases defined in Table 1 for a) acetone and b) ethanol.

Table 1 - Initial conditions and stability limits for acetone (A) and ethanol (E) cases.

Cases	N-AF2	N-AF6	N-AF8
U_j(m/s)	36	36	48
Re_g	21281	21281	28374
Q (g/min)	75	45	45
Re_l	6967	4180	4180
We	45	45	80
F/A (by mass)	0.37	0.22	0.17
U_j/U_{BO} @ Lr=80mm	0.49	0.56	0.75
U_j/U_{BO} @ Lr=25mm	0.54	0.63	0.84
U_j/U_{BO} @ Lr=0mm	0.68	-	-

Cases	N-EF2	N-EF6	N-EF8
U_j(m/s)	36	36	48
Re_g	21281	21281	28374
Q (g/min)	75	45	45
Re_l	19496	11698	11698
We	48	48	86
F/A (by mass)	0.37	0.22	0.17
U_j/U_{BO} @ Lr=80mm	0.48	0.56	0.75
U_j/U_{BO} @ Lr=25mm	0.57	0.60	0.80
U_j/U_{BO} @ Lr=10mm	0.63	0.64	0.86

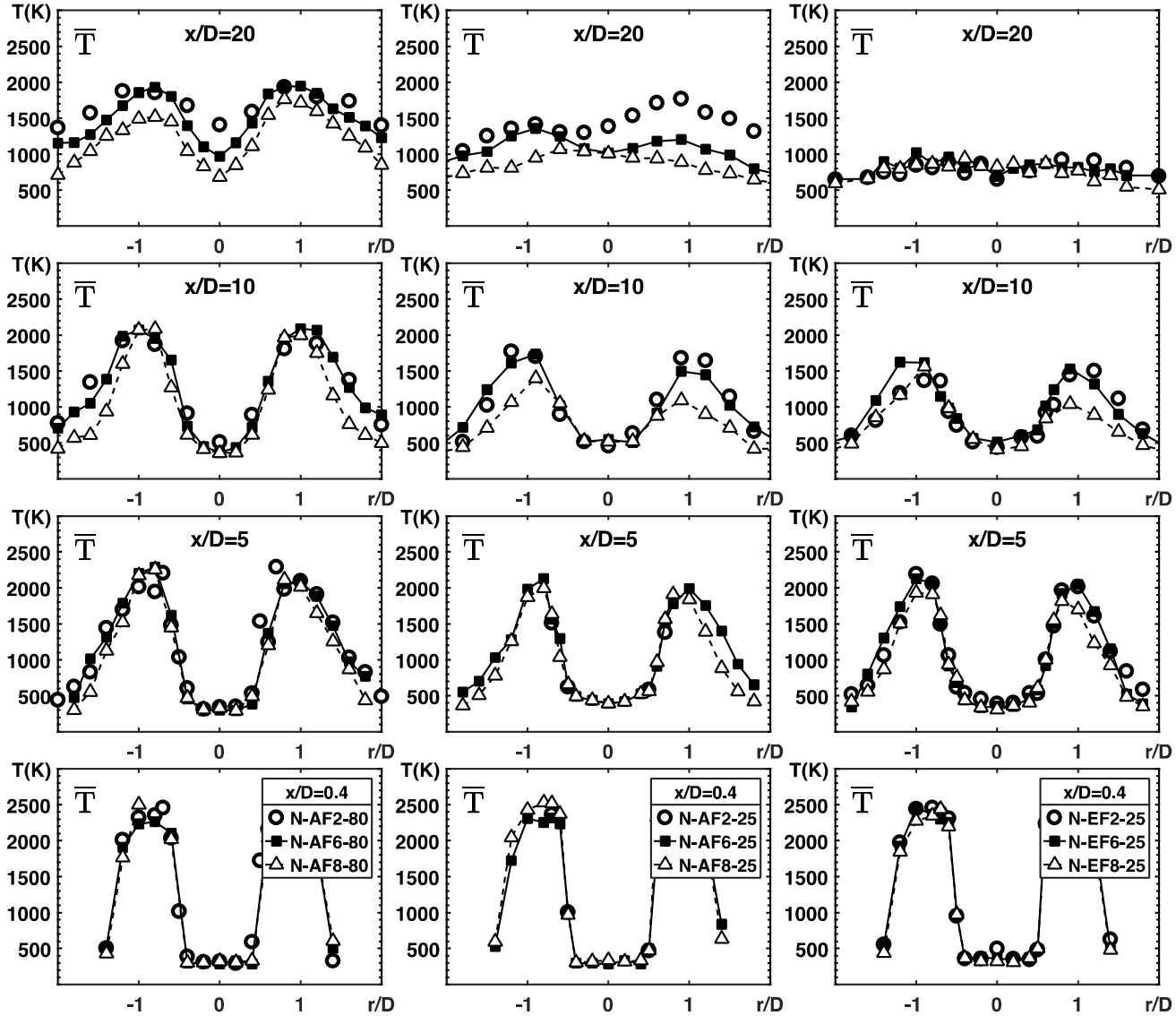

Fig. 3 – Radial profiles of the mean temperature measured at various axial locations using the CPP-fs-CARS system. Profiles are plotted for reacting acetone spray flames N-AF2, N-AF6 and N-AF8 comparing recess lengths 80 and 25mm. $T_{ad,C3H6O}$ = 2281K and $T_{ad,3GP}$ = 2512K. Alternatively, reacting ethanol spray flames N-EF2, N-EF6 and N-EF8 for recess length 25mm. $T_{ad,C2H6O}$ = 2355K and $T_{ad,3GP}$ = 2493K.

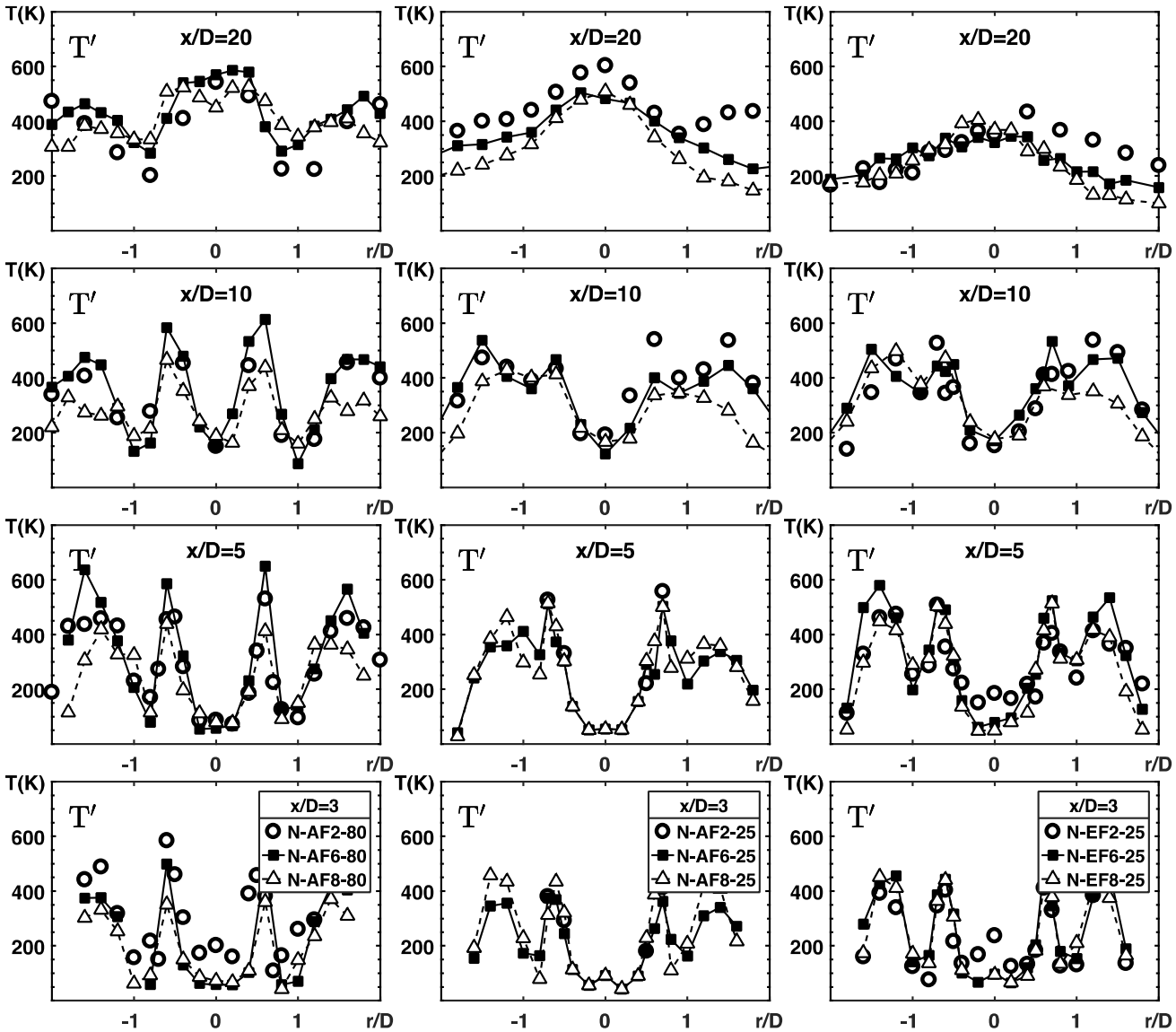

Fig. 4 – Radial profiles of the rms of temperature measured at various axial locations using the CPP-fs-CARS system. Profiles are plotted for reacting acetone spray flames N-AF2, N-AF6 and N-AF8 comparing recess lengths 80 and 25mm. $T_{ad,C3H6O}$ = 2281K and $T_{ad,3GP}$ = 2512K. Alternatively, reacting ethanol spray flames N-EF2, N-EF6 and N-EF8 for recess length 25mm. $T_{ad,C2H6O}$ = 2355K and $T_{ad,3GP}$ = 2493K.

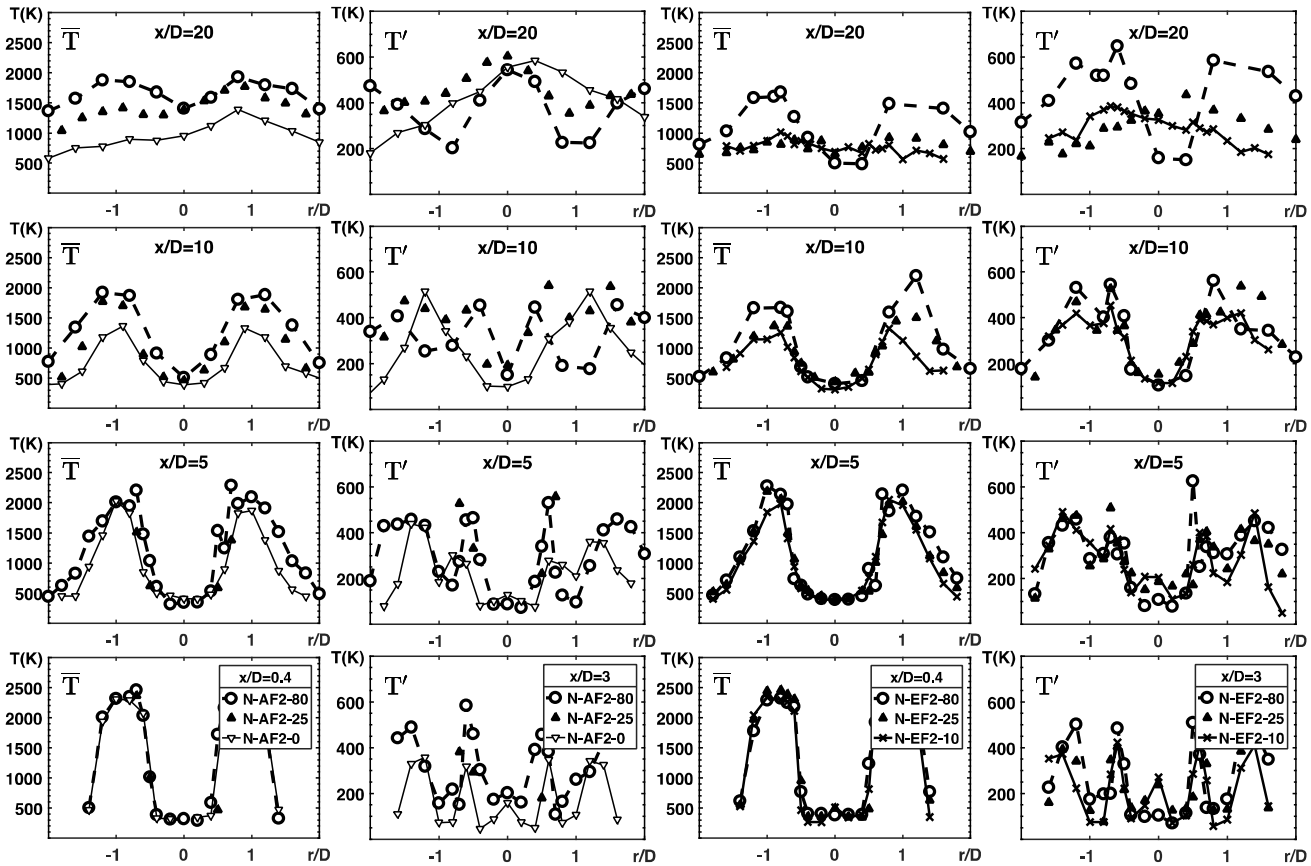

Fig. 5 – Radial profiles of the mean and rms of temperature measured at various axial locations using the CPP-fs-CARS system. Profiles are plotted for reacting acetone and ethanol spray flames comparing recess length N-AF2-80/N-EF2-80, N-AF2-25/N-EF2-25 and N-AF2-0/N-EF2-10. For acetone, $T_{ad,C3H6O}$ = 2281K and $T_{ad,3GP}$ = 2512K; for ethanol, $T_{ad,C2H6O}$ = 2355K and $T_{ad,3GP}$ = 2493K.

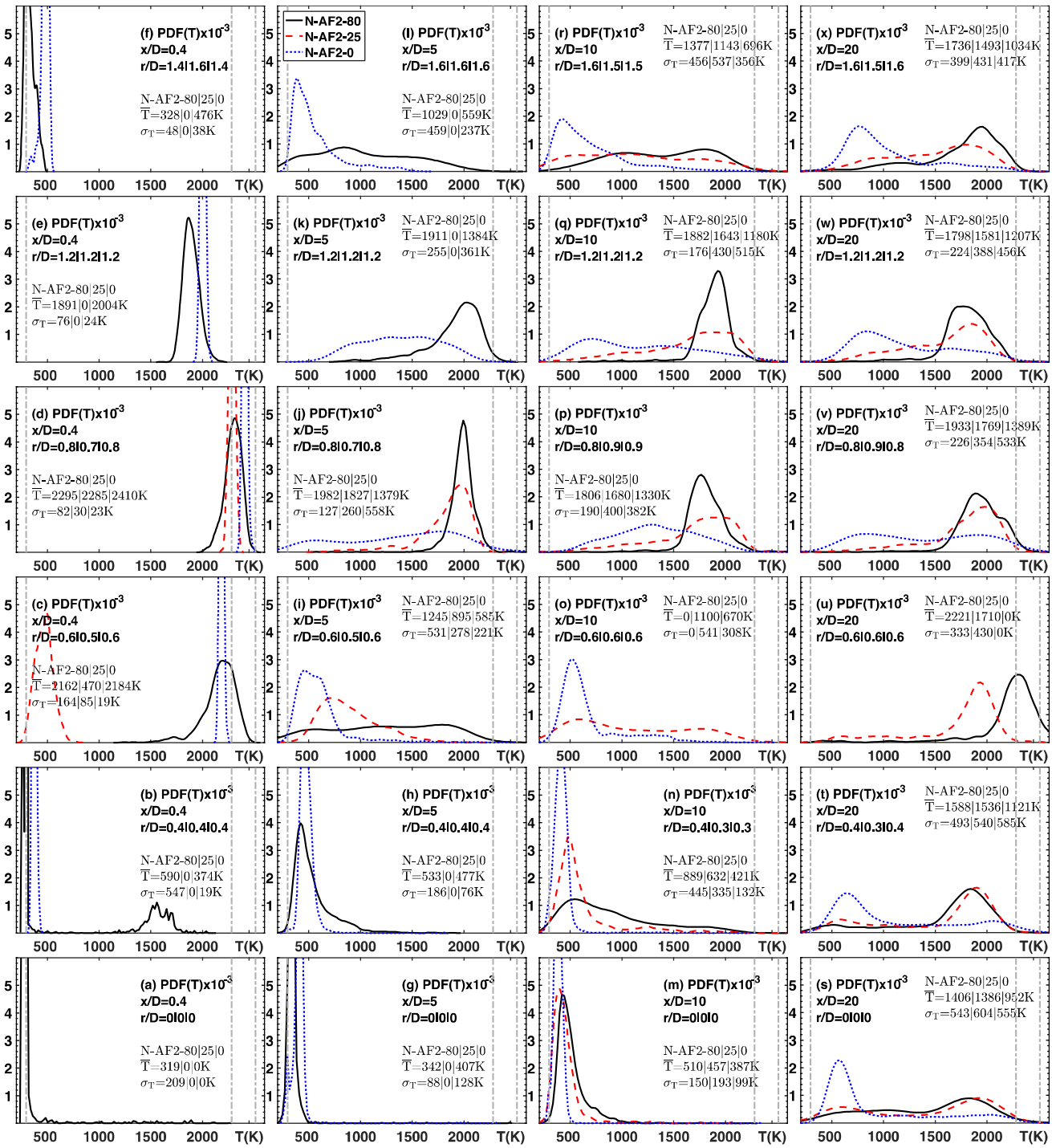

Fig. 6 – Spatial mapping of temperature PDF(T) using the CPP-fs-CARS for N-AF2-80 (solid), N-AF2-25 (dash) and N-AF2-0 (dot). Room temperature, $T_{ad,C3H6O}$ = 2281K and $T_{ad,3GP}$ = 2512K demarcated as vertical lines.

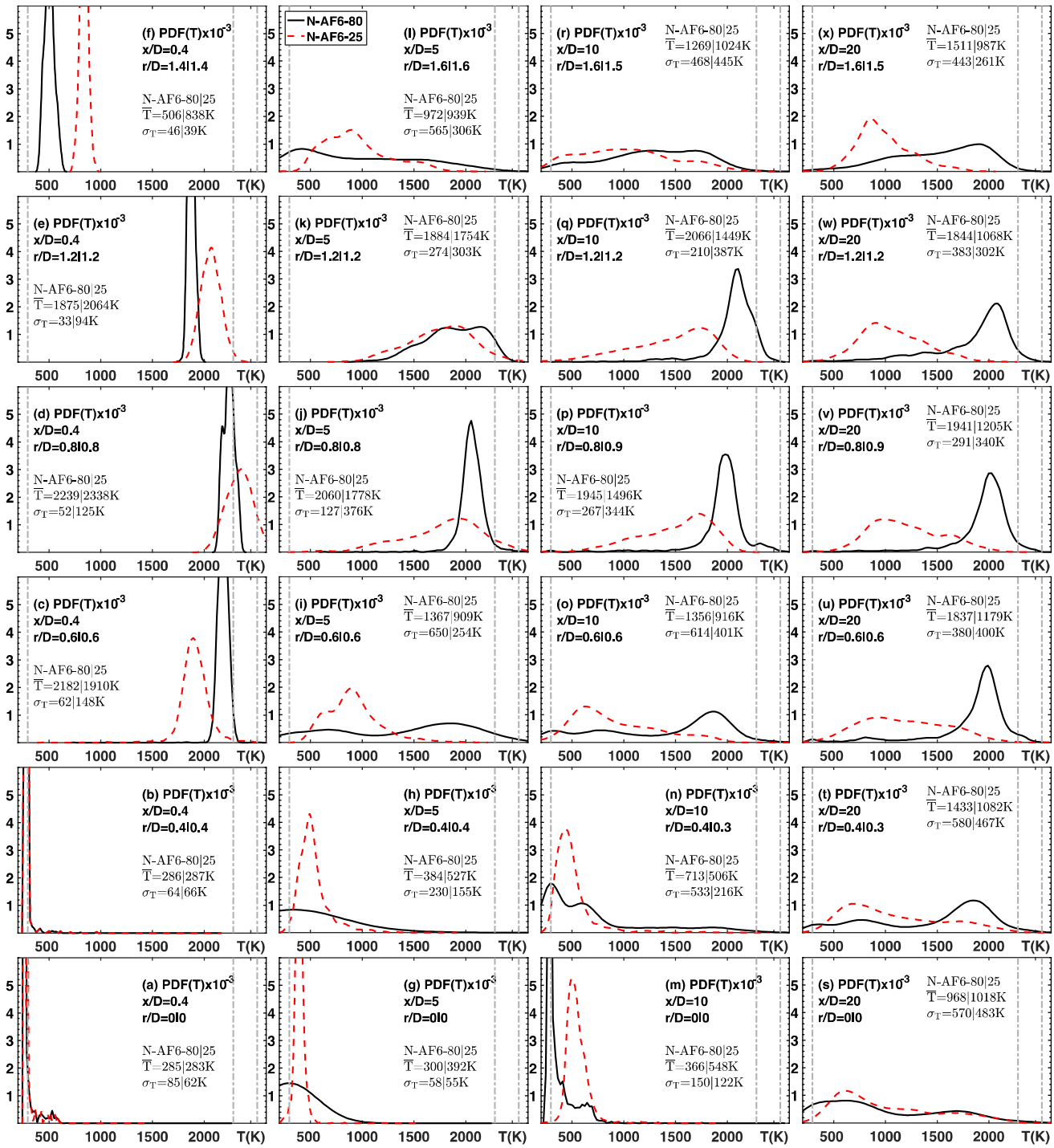

Fig. 7 – Spatial mapping of temperature PDF(T) using the CPP-fs-CARS for N-AF6-80 (solid) and N-AF6-25 (dash). Room temperature, $T_{ad,C3H6O}$ = 2281K and $T_{ad,3GP}$ = 2512K demarcated as vertical lines.

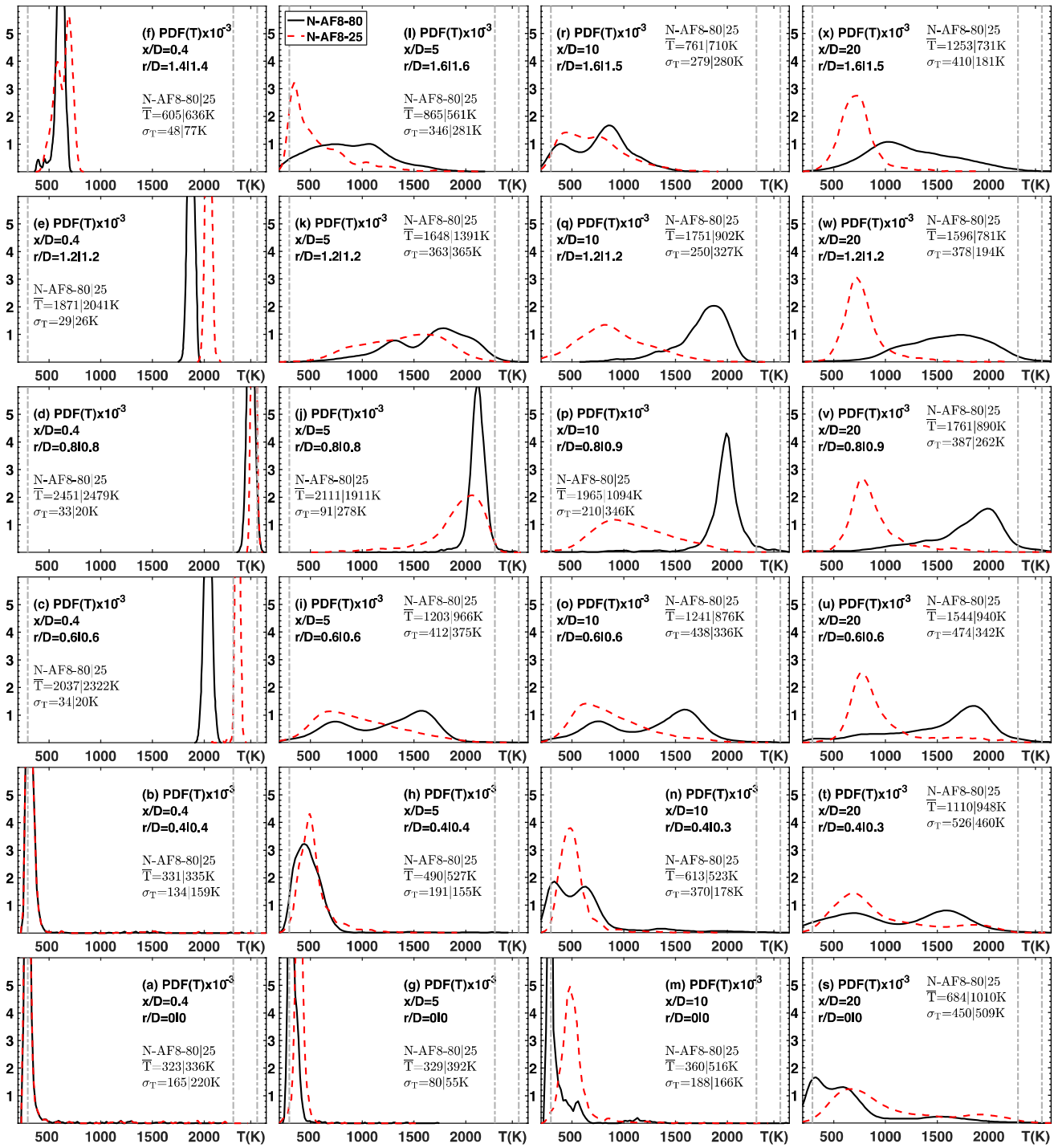

Fig. 8 – Spatial mapping of temperature PDF(T) using the CPP-fs-CARS for N-AF8-80 (solid) and N-AF8-25 (dash). Room temperature, $T_{ad,C3H6O}$ = 2281K and $T_{ad,3GP}$ = 2512K demarcated as vertical lines.

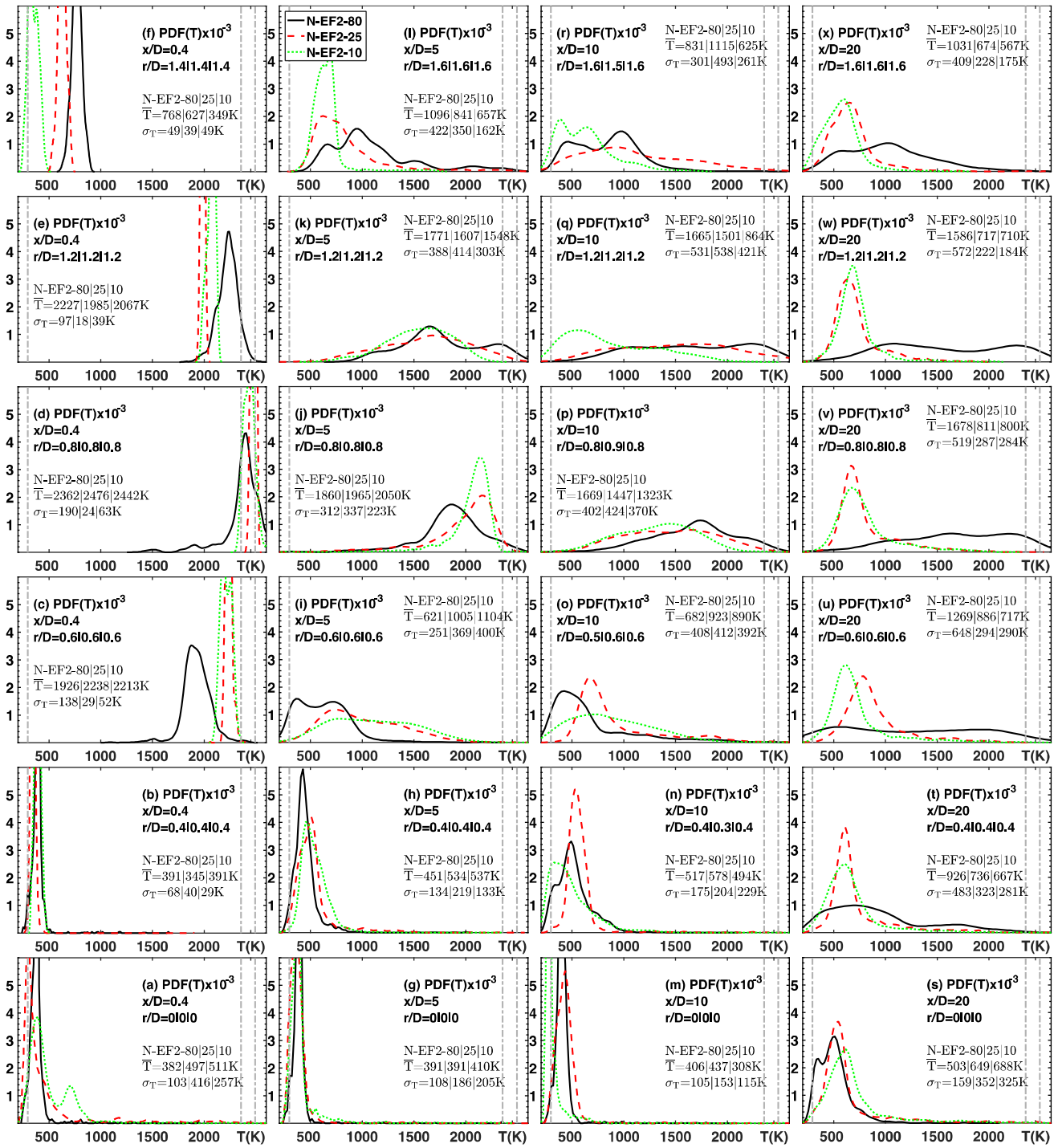

Fig. 9 – Spatial mapping of temperature PDF(T) using the CPP-fs-CARS for N-EF2-80 (solid), N-EF2-25 (dash) and N-EF2-10 (dot). Room temperature, $T_{ad,C2H6O}$ = 2355K and $T_{ad,3GP}$ = 2493K demarcated as vertical lines.

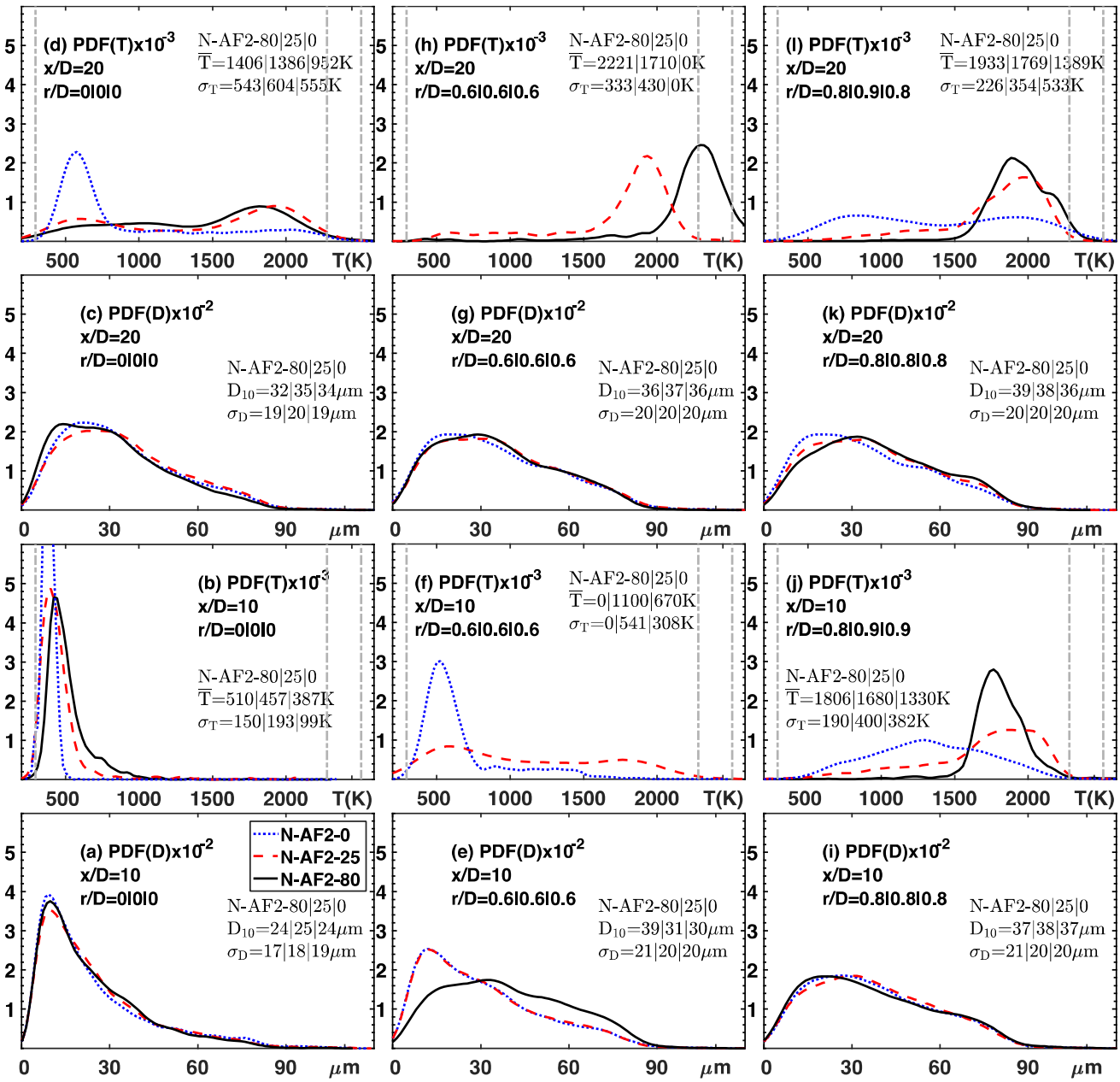

Fig. 10 – Temperature, PDF(T) and flow-field PDF(D) correlation for N-AF2-80 (solid), N-AF2-25 (dash) and N-AF2-0 (dot). Room temperature, $T_{ad,C3H6O}$ = 2281K and $T_{ad,3GP}$ = 2512K demarcated as vertical lines.

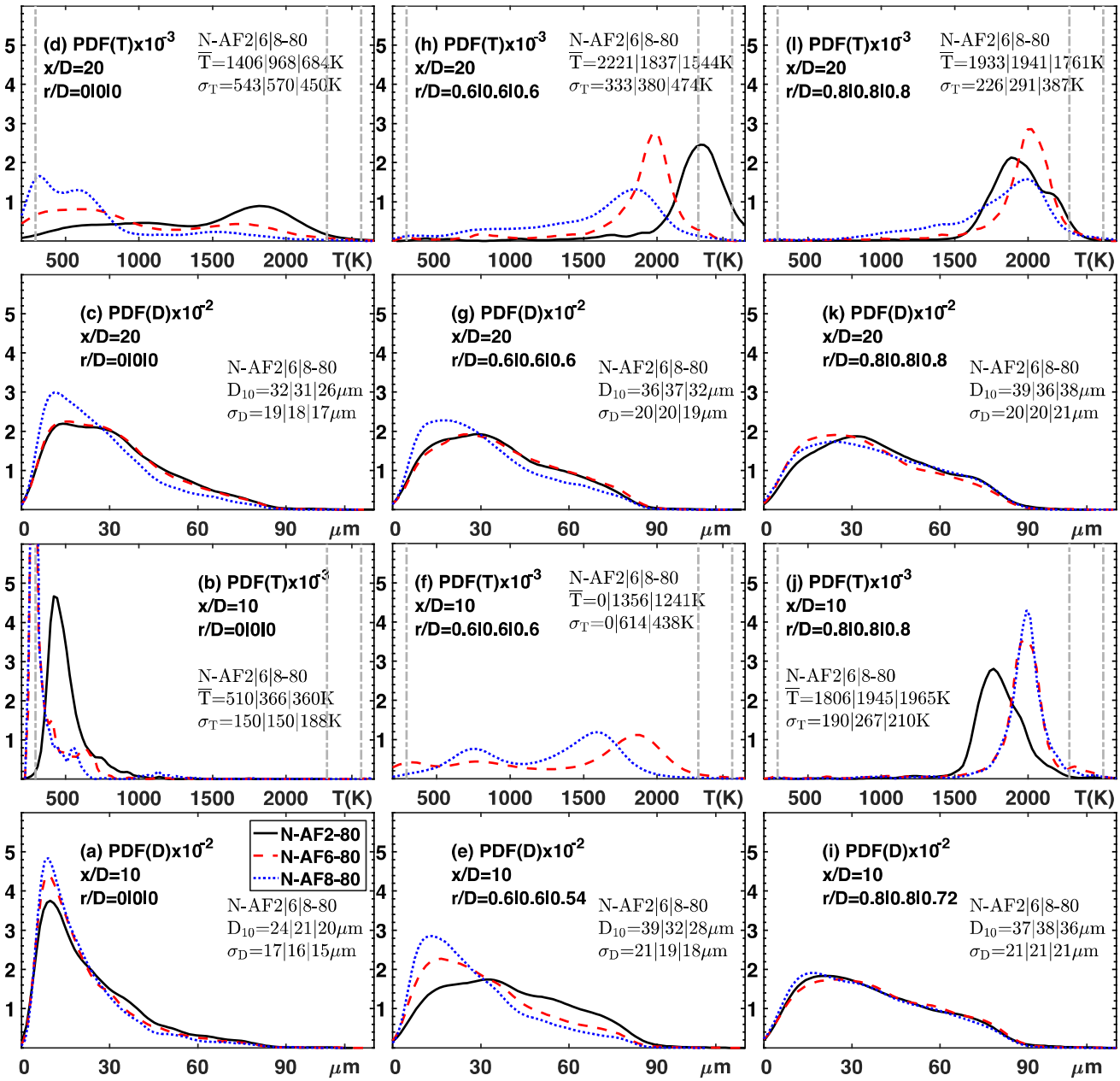

Fig. 11 – Temperature, PDF(T) and flow-field PDF(D) correlation for N-AF2-80 (solid), N-AF6-80 (dash) and N-AF8-80 (dot). Room temperature, $T_{ad,C3H6O}$ = 2281K and $T_{ad,3GP}$ = 2512K demarcated as vertical lines.

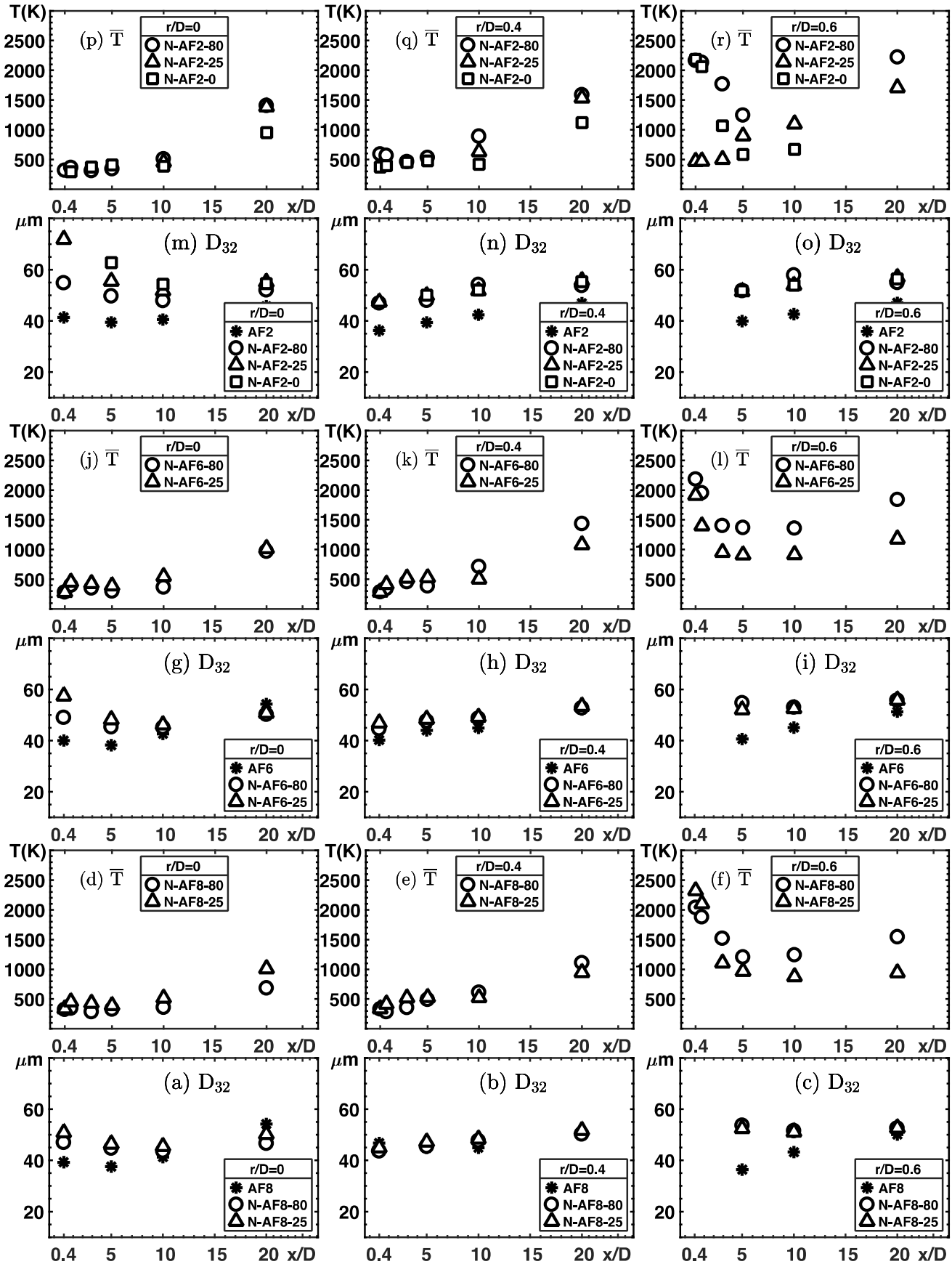

Fig. 12 – Axial profiles at r/D=0, 0.4 and 0.6 (left, middle, right columns respectively) of the mean temperature ($\overline{T}$, 1st, 3rd, 5th rows from top) measured using the CPP-fs-CARS system and Sauter mean diameter (D_{32}, 2nd, 4th, 6th row) measured using the PDA system. Profiles are plotted for reacting acetone spray flames comparing recess lengths. For acetone, $T_{ad,C3H6O}$ = 2281K and $T_{ad,3GP}$ = 2512K.